The Cryosphere

Open Access

Sea ice pCO$_2$ dynamics and air–ice CO$_2$ fluxes during the Sea Ice Mass Balance in the Antarctic (SIMBA) experiment – Bellingshausen Sea, Antarctica

N.-X. Geilfus[1,2,3], **J.-L. Tison**[2], **S. F. Ackley**[4], **R. J. Galley**[5], **S. Rysgaard**[1,5,6], **L. A. Miller**[7], and **B. Delille**[3]

[1]Arctic Research Centre, Aarhus University, Aarhus, Denmark
[2]Laboratoire de Glaciologie, Université Libre de Bruxelles, Brusells, Belgium
[3]Unité d'Océanographie Chimique, Université de Liège, Liège, Belgium
[4]Department of Geological Sciences, University of Texas at San Antonio, San Antonio, TX, USA
[5]Centre for Earth Observation Science, University of Manitoba, Winnipeg, Canada
[6]Greenland Climate Research Centre, Greenland Institute of Natural Resources, Nuuk, Greenland
[7]Centre for Ocean Climate Chemistry, Institute of Ocean Sciences, Fisheries and Oceans, Canada, Sidney, BC, Canada

Correspondence to: N.-X. Geilfus (geilfus@bios.au.dk)

Abstract. Temporal evolution of pCO$_2$ profiles in sea ice in the Bellingshausen Sea, Antarctica, in October 2007 shows physical and thermodynamic processes controls the CO$_2$ system in the ice. During the survey, cyclical warming and cooling strongly influenced the physical, chemical, and thermodynamic properties of the ice cover. Two sampling sites with contrasting characteristics of ice and snow thickness were sampled: one had little snow accumulation (from 8 to 25 cm) and larger temperature and salinity variations than the second site, where the snow cover was up to 38 cm thick and therefore better insulated the underlying sea ice. We show that each cooling/warming event was associated with an increase/decrease in the brine salinity, total alkalinity (TA), total dissolved inorganic carbon (TCO$_2$), and in situ brine and bulk ice CO$_2$ partial pressures (pCO$_2$). Thicker snow covers reduced the amplitude of these changes: snow cover influences the sea ice carbonate system by modulating the temperature and therefore the salinity of the sea ice cover. Results indicate that pCO$_2$ was undersaturated with respect to the atmosphere both in the in situ bulk ice (from 10 to 193 µatm) and brine (from 65 to 293 µatm), causing the sea ice to act as a sink for atmospheric CO$_2$ (up to 2.9 mmol m^{-2} d^{-1}), despite supersaturation of the underlying seawater (up to 462 µatm).

1 Introduction

Sea ice formation and melting may have a strong impact on the carbon cycle of polar oceans (e.g., Rysgaard et al., 2011; Delille et al., 2014). However, processes related to freezing and melting of sea ice, as well as their impact on CO$_2$ exchanges with the atmosphere, are still poorly understood (Parmentier et al., 2013). Detailed studies have been conducted on sea ice inorganic carbon chemistry and the impact of sea ice on the carbon cycle and the CO$_2$ exchanges between atmosphere, sea ice, and the ocean over the last decade (Semiletov et al., 2004; Zemmelink et al., 2006; Rysgaard et al., 2007, 2011, 2012; Delille et al., 2007, 2014; Miller et al., 2011; Papakyriakou and Miller, 2011; Geilfus et al., 2012a, 2013; Nomura et al., 2010a, 2013). These studies have shown that, in both hemispheres, CO$_2$–carbonate chemistry in sea ice and brine is heterogeneous and variable, resulting in complex CO$_2$ dynamics.

The CO$_2$ chemistry of sea ice seems to be highly dependent on brine salinity, which is controlled by ice temperature (Weeks, 2010). Both brine concentration during ice growth and brine dilution during ice melt play major roles in the carbonate system dynamics within sea ice (Papadimitriou et al., 2004; Nomura et al., 2010a; Geilfus et al., 2012a). In parallel, temperature dependence of both the dissociation constants of the carbonate system and the Henry's law constant for CO$_2$

affect pCO$_2$ in sea ice. Brine concentration/dilution can be associated with precipitation/dissolution of calcium carbonate within the sea ice, also promoting an increase/decrease in the in situ brine pCO$_2$ (Papadimitriou et al., 2004, 2007; Rysgaard et al., 2007, 2012, 2014; Geilfus et al., 2012a, 2013). Primary production and respiration can also affect the CO$_2$–carbonate system within sea ice (Thomas and Dieckmann, 2010; Dieckmann and Hellmer, 2010; Delille et al., 2007). Finally, brine and gas transport within sea ice and across the air–ice and ice–water interfaces affect TA, TCO$_2$, and CO$_2$ distributions within the ice, together with the overall amount of CO$_2$ in the sea ice. The role of ice-covered oceans in the CO$_2$ balance has been largely ignored because continuous sea ice cover is assumed to impede gaseous exchange with the atmosphere. However, recent studies show that sea ice may mediate the air-to-sea CO$_2$ transfer. Understanding of the seasonal and geographical conditions of the inorganic carbon dynamics related to sea ice is limited. The main goal of this study is to add to the still limited database on inorganic carbon dynamic in ice-covered seas.

Although snow thickness and distribution are variable and primarily result from wind-induced redistribution during storms (Weeks, 2010), the impact of snow cover on the thermal evolution of sea ice can be significant (Massom et al., 2001). Snow, which has a low thermal conductivity compared to sea ice (Massom et al., 2001), provides thermal insulation between the cold air and the ice. The presence of a thick snow cover also affects the isostatic balance, potentially resulting in negative freeboard (i.e., the snow–ice interface is submerged below the seawater level). If the sea ice is permeable throughout the entire ice column, negative freeboard causes vertical flooding to at least the snow–ice interface through open brine channels. The percolation threshold above which columnar sea ice is considered permeable to fluid transport corresponds to a brine volume (which is controlled by temperature and salinity) of 5 % (Golden et al., 1998, 2007).

Therefore, snow accumulation could impact the CO$_2$–carbonate system within sea ice by regulating the ice temperature and the extent of flooding. The impact of snow on the CO$_2$ exchanges between sea ice and the atmosphere has previously been discussed by Nomura et al. (2010b); these authors suggested that a snow cover thicker than 9 cm could prevent any sea-ice–atmosphere exchanges of CO$_2$ and that melting snow can act as a physical barrier to CO$_2$ fluxes.

In this study, we examine the temporal evolution of in situ brine and bulk ice pCO$_2$ profiles associated with physical and biogeochemical variables in the sea ice cover of two contrasting study sites, named "Brussels" and "Liège" between 1 and 23 October 2007, during the Sea Ice Mass Balance in the Antarctic (SIMBA) cruise (Bellingshausen Sea, Antarctica) (Fig. 1) (Lewis et al., 2011). Further, we differentiate the dynamics of in situ brine and bulk ice pCO$_2$. Sea ice temperature and bulk salinity differences at these two stations, in part due to substantial difference in snow cover, impact the
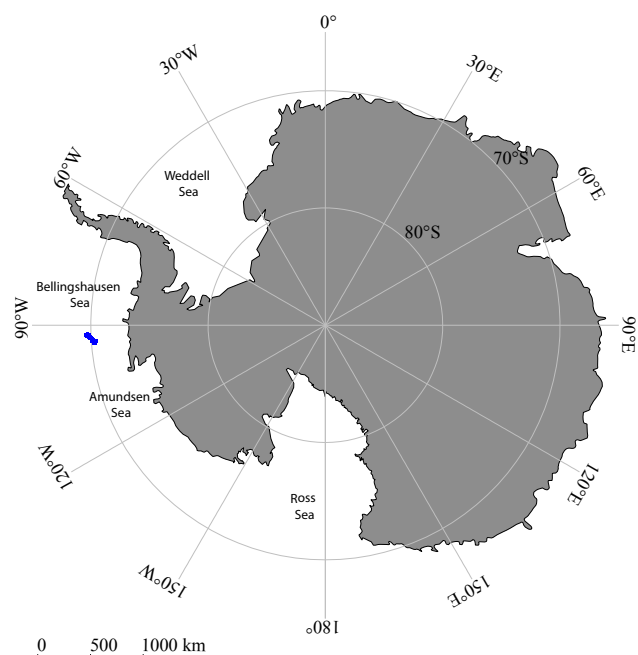

Figure 1. Location of the sampling area for the SIMBA cruise 2007 (blue patch), in the Bellingshausen Sea, Antarctica.

inorganic carbon dynamics within sea ice and its brine and the related air–ice CO$_2$ fluxes.

2 Study site, materials, and methods

2.1 Selection of study site

The SIMBA cruise investigated the physical and biological interactions between the ocean, sea ice, snow cover, and atmosphere in the Bellingshausen Sea, onboard the R/V *Nathaniel B. Palmer* (NBP) in October 2007. During this $\sim$ 1-month experiment, the vessel was moored to a first-year sea-ice floe, the Ice Station Belgica (ISB), south of Peter I Island, at approximately 69–71° S and 90–95° W (Fig. 1). The station was chosen for its wide variety of ice types and snow cover (Lewis et al., 2011), characteristic of the greater region, and the size of the ice floe ($\sim$ 5 km^2) was deemed large enough to survive the duration of the field experiment. Sampling was conducted at two distinct sites based on (i) homogeneity of the surface properties within each site, to reduce within-site spatial variability; (ii) the contrast in ice and snow properties between the two chosen sites; and (iii) maximum distance from the ship (0.8 and 1.1 km), to prevent sample contamination. Each site was 100 m × 60 m and subdivided into small work sub-areas approximately 5 m × 5 m. The 25 m^2 sub-areas were located adjacent to each other to minimize spatial variability (Lewis et al., 2011). Each station was sampled at 5-day intervals: the Brussels site (low snow cover, at 0.8 km) was sampled on 1, 6, 11, 16, and 21 Octo-
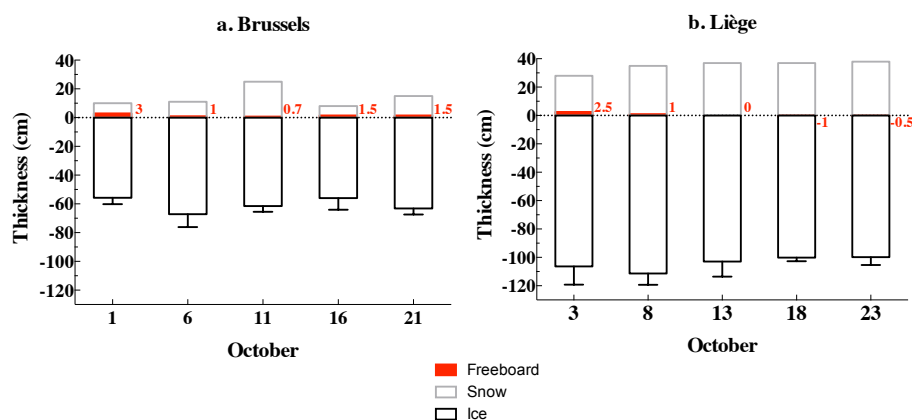
Figure 2. Ice (including range of observed values), snow thickness, and freeboard at the Brussels and Liège sites.

ber; the Liège site (high snow cover, at 1.1 km) was sampled on 3, 8, 13, 18, and 23 October (Fig. 2).

2.2 Sampling procedures

Ice cores were collected using an electro-polished stainless-steel corer (14 cm diameter) using an electric drill head, connected by a long cord to a power supply generator located downwind. Cores were immediately wrapped in polyethylene bags and placed in an insulated box filled with gel packs pre-cooled to −30 °C in order to limit brine drainage from samples (Tison et al., 2008) and brought back to the ship laboratory. Sackholes (Gleitz et al., 1995) for collecting brine were drilled to four depths: 15, 30, 40, and 50 cm at the Brussels site; and 15, 30, 60 and 90 cm at the Liège site. Each sackhole was covered with a plastic lid to prevent contamination by falling snow. Brine seeped into the sackholes for 10 to 60 min before collection using a peristaltic pump (Cole Palmer, Masterflex-Environmental Sampler). Under-ice seawater was collected using the same peristaltic pump, with the inlet positioned at the ice–water interface, and at 1 and 30 m depths. On each sampling date, ice cores, brine, and seawater were collected and analyzed for a full range of physical and biogeochemical variables: temperature (T), salinity (S), water stable isotopes of $\delta^{18}\text{O}$, chlorophyll a (Chl a), total alkalinity (TA), pH_T, and in situ CO_2 partial pressure ($p\text{CO}_2$). Brine samples for pH_T and TA analyses were only collected from the shallowest sackhole depth (at 0 to 15 cm) and at 0 to 40 cm depth at the Brussels site and 0 to 60 cm depth at the Liège site sackholes.

2.3 Materials and methods

The ice temperature was measured immediately after extraction of the ice core using a calibrated temperature probe (TESTO 720, ±0.1 °C precision) inserted into pre-drilled holes (∼ 5 cm intervals) perpendicular to the core sides. In the field, the ice core dedicated to bulk ice salinity measurements was cut into 5 cm thick slices which were stored in

separate, closed containers. These ice samples were melted at room temperature onboard, and bulk ice salinity on the practical salinity scale was determined from conductivity and temperature using a portable calibrated Orion 3-Star conductivity meter (precision of ±0.1). Samples with salinity higher than 42 were diluted with ultrapure water using an analytical balance. Brine volumes profiles were calculated for each core using these bulk ice salinities and ice temperatures according to Cox and Weeks (1983) for ice temperatures below −2 °C and according to Leppäranta and Manninen (1988) for ice temperatures within the range −2 to 0 °C. Calculated brine salinity profiles were determined from the in situ ice temperatures (after Cox and Weeks, 1983).

Aliquots (10 mL) of the bulk melted sea ice samples were transferred to gastight vials for $\delta^{18}\text{O}$ measurements at the Australian Antarctic Cooperative Research Centre (CRC). Isotope ratios were measured with a dual-inlet VG SIRA mass spectrometer using the conventional water–CO_2 equilibration method (accuracy with respect to VS-MOW = ±0.12 ‰).

The pH of the sea-ice brine and seawater was measured using a Metrohm combined electrode calibrated on the total hydrogen ion scale (pH_T) using TRIS (2-amino-2-hydroxymethyl-1.3-propanediol) and AMP (2-aminopyridine) buffers prepared at salinities of 35 and 75 according to the formulations proposed by DOE (1994). Samples were maintained as close as possible to their in situ temperature (typically below 3 °C), and measurements of pH_T were carried out as soon as possible upon return to the ship laboratory (typically less than 2 h after sampling). The pH electrode was calibrated at temperatures ranging from 0 to 4 °C and at salinities ranging from 35 to 75. The accuracy of the pH_T measurements was ±0.01 pH unit (Frankignoulle and Borges, 2001).

Total alkalinity in the brine and underlying seawater was measured by open-cell titration with HCl 0.1M, and the endpoints were determined according to Gran (1952). Routine analyses of Certified Reference Materials provided by

A. G. Dickson, Scripps Institution of Oceanography, verified that the error in these TA data was smaller than ± 4 μmol kg^{-1}. Total inorganic carbon (TCO$_2$) and pCO_2 (denoted as pCO_{2calc}) were calculated from TA and pH$_T$ using the CO$_2$ acidity constants of Mehrbach et al. (1973) refit by Dickson and Millero (1987) and other constants advocated by DOE (1994). We assumed that the CO$_2$ dissociation constants were applicable at subzero temperatures as suggested by Marion (2001) and Delille et al. (2007).

Brine and underlying seawater pCO_2 were measured in situ using a custom-made equilibration system (Geilfus et al., 2012a). The system consisted of a membrane contactor equilibrator (Membrana, Liqui-cell) connected to a non-dispersive infrared gas analyzer (IRGA, Li-Cor 6262) via a closed air loop. Brine and airflow rates from the equilibrator and IRGA were approximately 2 and 3 L min^{-1}, respectively. Temperature was measured within the sackholes or under-ice water and at the equilibrator outlet simultaneously using Li-Cor temperature sensors. The pCO_2 values were temperature-corrected assuming that the Copin Montégut (1988) relation is valid at low temperatures and high salinities. The IRGA was calibrated immediately upon returning to the ship while the analyzer was still cold. All devices, except the peristaltic pump, were enclosed in an insulated box that contained a 12 V power source providing enough heat to keep the inside temperature just above 0 °C.

Ice cores were kept frozen during storage and shipping for subsequent analysis of bulk ice pCO_2 at the Laboratoire de Glaciologie, Université Libre de Bruxelles, Belgium. The general principle of the method was to equilibrate the sea ice samples at the in situ temperature with a mixture of N$_2$ and CO$_2$ at known concentrations (so-called standard gas, 396 µatm) and rapidly extract the gas into a Varian 3300 gas chromatograph under vacuum (Geilfus et al., 2012b). Each ice sample was cut into a 4 cm $\times$ 4 cm $\times$ 4.5 cm cube to tightly fit the equilibration container, thereby both minimizing the headspace and keeping it consistent. The standard gas was injected at 1013 mbar into the equilibration container containing the ice sample. Then the container with the ice sample was placed in a thermostatic bath setup at the field in situ temperature for 24 h. This timing was chosen to ensure that the sample is re-equilibrated to the brine volume and chemical conditions at the in situ temperature. A quick injection into the gas chromatograph then allowed the reconstruction of the equilibrium brine pCO_2 at the in situ temperature. This method is only valid if the ice is permeable at the in situ conditions (Geilfus et al., 2012b) and microstructure changes resulting from cooling during storage and warming prior to analysis are assumed to have a minor impact on the bulk ice pCO_2.

Air–ice CO$_2$ fluxes were measured using an accumulation chamber (West System) placed on top of the ice. The chamber was a metal cylinder closed at the top, with an internal diameter of 20 cm and an internal height of 9.7 cm. A rubber seal surrounded by a serrated steel edge ensured an airtight
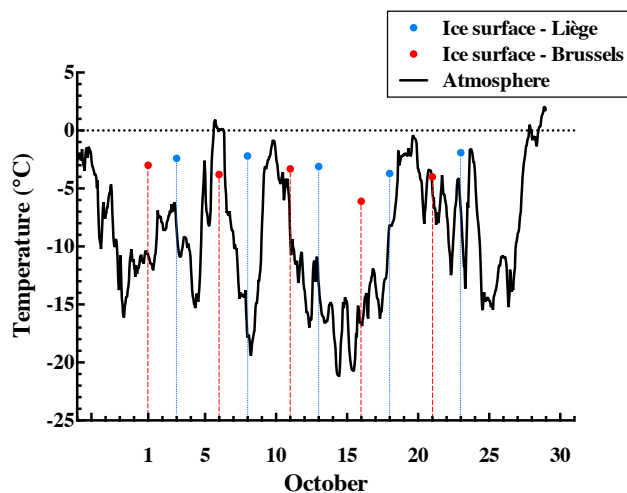

Figure 3. Daily time series of air temperature (°C) recorded on the ship and the surface ice temperature of the different sampling stations at the Brussels (red dots) and Liège (blue dots) sites.

connection between the ice and the chamber. Over snow, a steel tube was mounted at the base of the chamber to enclose the snowpack to the ice surface and prevent lateral infiltration of air into the chambered volume of snow. The chamber was connected in a closed loop to the IRGA with an air pump rate of 3 L min^{-1}. The pCO_2 in the chamber was recorded every 30 s for a minimum of 5 min. The flux was computed from the slope of the linear regression of pCO_2 versus time ($r^2 > 0.99$) according to Frankignoulle (1988), taking into account the volume of ice or snow enclosed within the chamber. The average uncertainty of the flux computation due to the standard error of the regression slope was ± 3 %.

3 Results

3.1 Atmospheric conditions

During the 2007 winter–spring transition in the Bellingshausen Sea, several low-pressure systems of varying intensity and length occurred at the sampling location. Fluctuations in the air temperature are shown in Fig. 3, along with the surface ice temperature measured at each station. At least three successive cycles of warming and cooling were recorded with air temperatures ranging from 0.5 to -20 °C. These cycles consisted of warm atmospheric fronts from the north, generally accompanied by high-velocity winds and precipitation, followed by cold air temperatures and little precipitation (Lewis et al., 2011; Vancoppenolle et al., 2011).

3.2 Sea ice and snow conditions

The Brussels and Liège sites had contrasting conditions in snow, ice thickness (Fig. 2), and ice texture, which are presented in detail by Lewis et al. (2011).
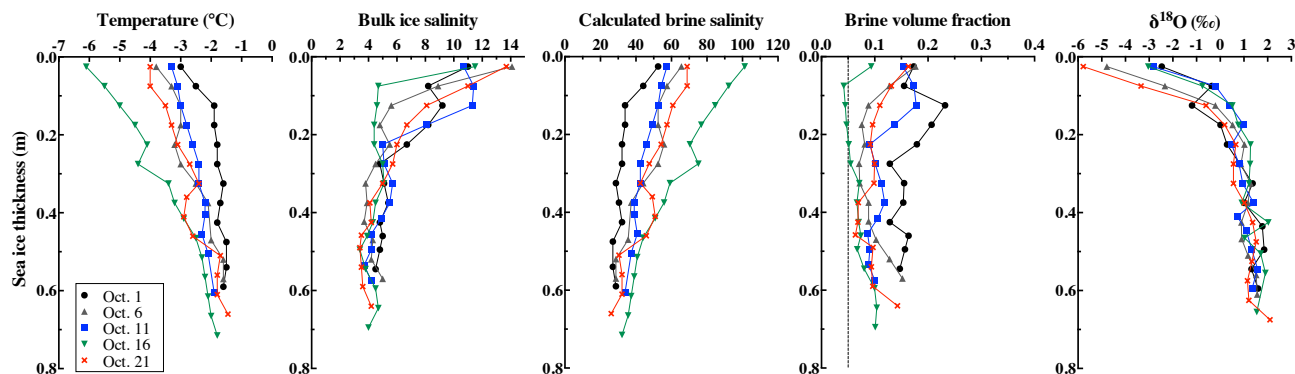
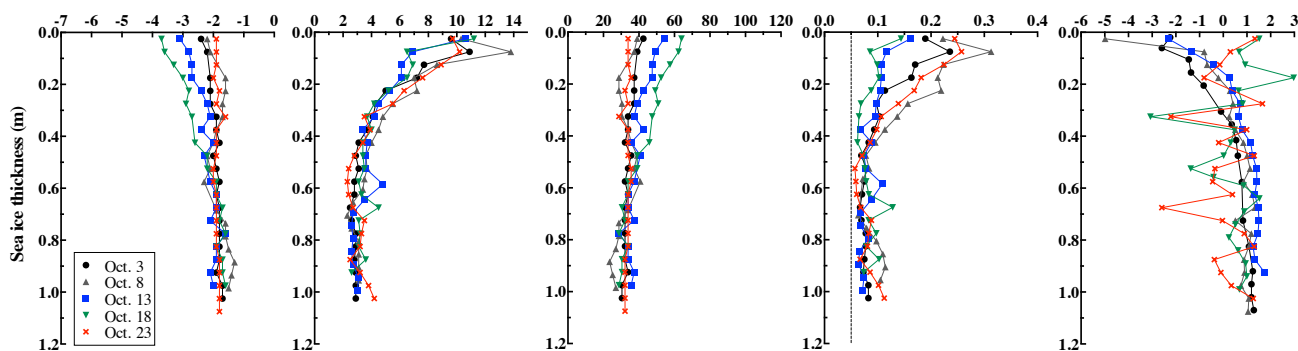**Figure 4.** Profiles of temperature (°C), bulk ice salinity, calculated brine salinity, brine volume fraction, and ^{18}O isotopic ratio from the Brussels (top panels) and Liège (bottom panels) sites.

At the Brussels site, the ice thickness, as determined by coring, ranged from 55 to 67 cm, while the snow cover ranged from 8 to 25 cm (Fig. 2a). The ice freeboard was positive and ranged from 0.7 to 3 cm. The ice cover was mainly composed of columnar crystals (Lewis et al., 2011). The ice temperatures ranged from −1.5 to −6.1 °C (Fig. 4). The main changes in temperatures were observed in the top 40 cm of the ice cover, oscillating between cooling and warming events within a 1 °C temperature window (from −3 to −4 °C), except on 16 October, when the near-surface ice temperature decreased to −6.1 °C and the top 40 cm reached its minimum observed temperature. The bulk ice salinity ranged from 3.4 to 14.1. The profiles were typically S-shaped, as described by Eicken (1992), with higher salinities (from 11.5 to 14.1) in the top layer, dropping to minimum values (on average, $S = 4.1$) at the bottom. Between 1 and 16 October, the brine salinities increased from the bottom to the top of the ice cover, with values close to seawater ($S = 34$) at the bottom to a maximum of 101 at the top on 16 October. The brine volume was always greater than 5 %, except in the top 20 cm of the ice cover on 16 October. The $\delta^{18}O$ isotopic ratio ranged from −5.8 to 2.1 ‰. The top 15 cm showed negative $\delta^{18}O$ values at each sample interval, while the rest of the pro-

file was increasing steadily towards a value of +2 ‰ at the bottom.

At the Liège site, the ice and snow cover were thicker than at the Brussels site and ranged from 99 to 106 cm and from 28 to 38 cm, respectively (Fig. 2b). The ice freeboard was negative on 18 and 23 October, flooding the snow–ice interface. The ice cover at the Liège site was mainly composed of granular sea ice with inclusions of columnar and snow ice layers at different levels in the ice profile (see Lewis et al., 2011, for a detailed description of the ice texture profile at the Liège site). These inclusions, associated with sharp excursions in the $\delta^{18}O$ ratios (Fig. 4), indicate a history of dynamic conditions and repeated subsequent rafting events (Lewis et al., 2011). The observed variations of the bulk ice temperature and salinity, as well as the calculated brine salinity, were smaller than those observed at Brussels (Fig. 4). The ice temperature ranged from −1.3 to −3.7 °C. The ice cover showed similar warm and isothermal profiles on 3, 8, and 23 October, with brine salinities close to seawater values throughout the ice column. The ice cover cooled from 8 to 18 October, when the minimum temperature and maximum brine salinity were observed, as we also observed at the Brussels site. The bulk ice salinity ranged from 2.3 to 13.8, and the salinity profiles were also typically S-shaped, with the top layer rang-
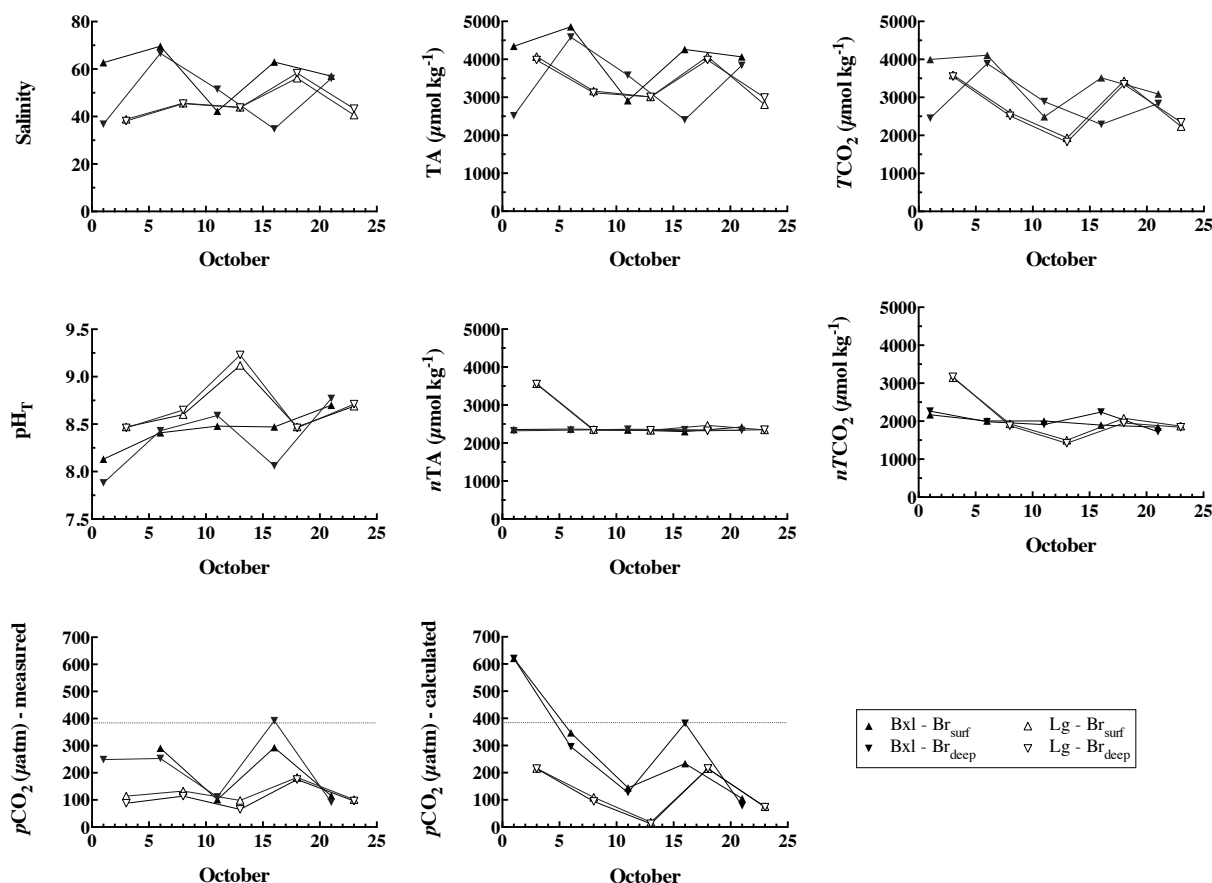
Figure 5. Evolution of salinity, pH$_T$, TA (in µmol kg^{-1}), nTA (TA normalized to a salinity of 34, in µmol kg^{-1}), calculated TCO$_2$ (in µmol kg^{-1}) and $n$$TCO_2$ (TCO$_2$ normalized to a salinity of 34, in µmol kg^{-1}), and measured and calculated pCO$_2$ (in µatm) in surface and deep brine sackholes from the Brussels (Bxl) and Liège (Lg) sites. The dotted line represents the atmospheric pCO$_2$ in October 2007.

ing from 6.5 to 13.8, while the average salinity of the bottom layer was 3. The calculated brine volume fraction was always above 5 %. The δ^{18}O ratios ranged from −4.9 to 2.9 ‰. At the top of the ice, δ^{18}O was negative from 3 to 13 October and positive on our last 2 sampling days. In the lower half of the profiles, δ^{18}O values were generally around 1 ‰, although the cores sampled on 18 and 23 October had negative δ^{18}O intervals, further indicative of ice rafting.

3.3 Carbonate system

At the Brussels site, TA in brine sampled from sackholes ranged from 2406 to 4855 µmol kg^{-1}, while TCO$_2$ ranged from 2288 to 4110 µmol kg^{-1} (Fig. 5). Changes in TA and TCO$_2$ closely mimicked the salinity changes. Normalizing TA and TCO$_2$ to a salinity of 34 (denoted as nTA and $n$$TCO_2$) indicate the sensitivity of these parameters to salinity changes; both nTA and $n$$TCO_2$ remain relatively stable (2350 and 2010 µmol kg^{-1}, respectively). The pH$_T$ ranged from 7.9 to 8.8 and increased continuously during the survey, except for a significant decrease in the deeper brine on 16 October (Fig. 5) associated with decreased brine salinity

and TA. The in situ brine pCO$_2$ ranged from 82 to 392 µatm. Brine was undersaturated in CO$_2$ relative to the atmosphere (383.8 µatm in 2007), except on 16 October (Figs. 5 and 6). The brine pCO$_{2calc}$ was similar to brine pCO$_2$ measured in situ (± 50 µatm), except on 1 October when brine pCO$_{2calc}$ was extremely high (620 µatm, Fig. 5). From 1 to 6 October, the in situ brine pCO$_2$ values were from 210 to 271 µatm (Fig. 6). Then, the in situ brine pCO$_2$ decreased on 11 October and increased again on 16 October to concentrations ranging from 248 to 392 µatm. On 21 October, the in situ brine pCO$_2$ decreased down to concentrations ranging from 82 to 115 µatm. The bulk ice pCO$_2$ ranged from 15 to 150 µatm (Fig. 6), generally increasing with depth and lower or equal to the brine pCO$_2$.

At the Liège site, the brine salinity ranged from 38.1 to 58.3. TA ranged from 2806 to 4074 µmol kg^{-1}, while TCO$_2$ ranged from 1826 to 3590 µmol kg^{-1} (Fig. 5). As for the Brussels site, TA and TCO$_2$ changes seem closely related to salinity changes, except on 3 October. The pH$_T$ ranged from 8.5 to 8.7 with a significant increase on 13 October to a maximum of 9.2 (Fig. 5). The in situ brine pCO$_2$ was un-
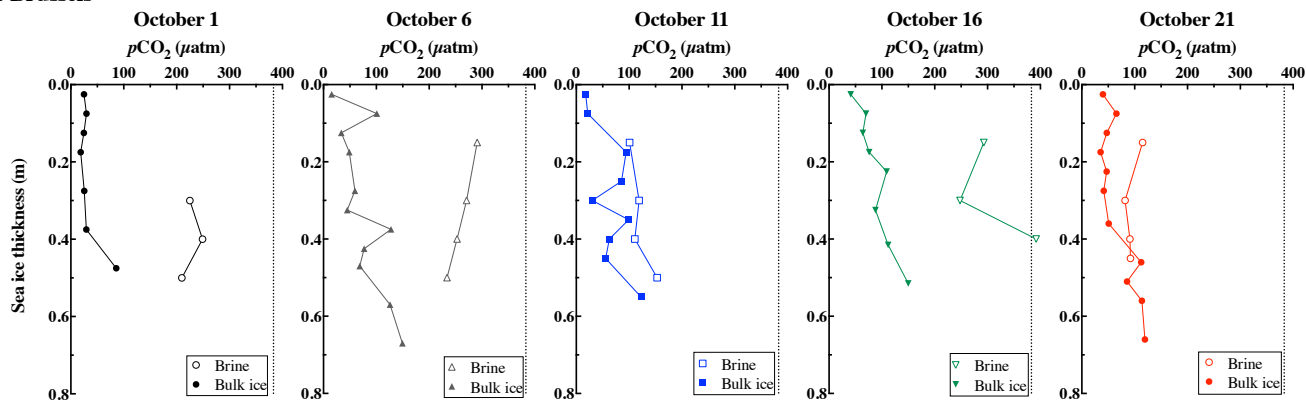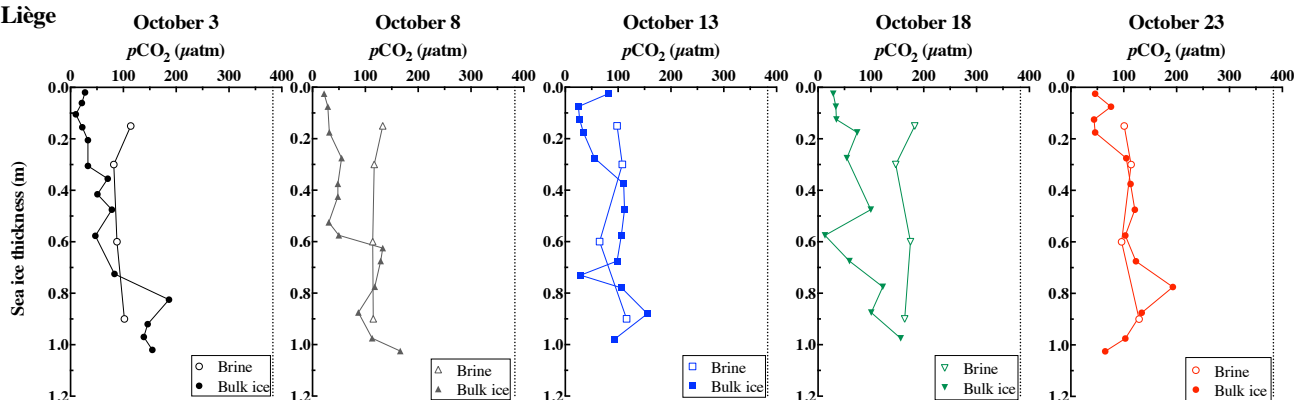
Figure 6. Vertical profiles of the in situ brine $p\text{CO}_2$ (in µatm) and bulk ice $p\text{CO}_2$ (in µatm) from the Brussels (top panels) and Liège (bottom panels) sites. Data at 0.075–0.125 and 0.175 m depth of the station on 16 October were measured while the brine volume was 4.1–4.4 and 4.6 %, respectively.

dersaturated compared to the atmosphere, with values ranging from 65 to 183 µatm. These values were consistent with the brine $p\text{CO}_{2\text{calc}}$ (±80 µatm). Changes of the in situ brine $p\text{CO}_2$ were smaller than the variations at the Brussels site. The most significant change occurred on 18 October where the in situ brine $p\text{CO}_2$ increased to concentrations ranging from 147 to 183 µatm. The bulk ice $p\text{CO}_2$ ranged from 9 to 193 µatm (Fig. 6). Bulk ice $p\text{CO}_2$ were here generally more consistent with brine $p\text{CO}_2$, except in the colder stations on 8 and 18 October. The minimum concentrations were observed in the top 20 cm of the ice cover, while the maximum concentrations were observed at the sea ice interface with the underlying seawater. The mean bulk ice $p\text{CO}_2$ ranged from 70 to 79 µatm from 3 to 18 October and increased to 97 µatm on 23 October.

The salinity and CO_2 system parameters were relatively constant in the underlying seawater during our survey (Fig. 7). We observed a slight decrease in the salinity on 13 October, while pH_T decreased and $T\text{CO}_2$ increased on 11 and 13 October. The seawater $p\text{CO}_2$ measured in situ

was supersaturated relative to the atmosphere, ranging from 401 to 462 µatm.

3.4 Air–ice CO_2 fluxes

The CO_2 fluxes measured at the sea ice and snow interfaces with the atmosphere suggest that, except for a small efflux of $0.3\ \text{mmol m}^{-2}\ \text{d}^{-1}$ measured over the ice at the Brussels site on 16 October, both the sea ice and the snow acted as sinks for atmospheric CO_2 during our study (Fig. 8). In general, Brussels sea ice showed a small uptake of atmospheric CO_2 that was not significantly different from zero (Fig. 8a). At Liège, the uptake of atmospheric CO_2 was more substantial, ranging up to $-2.9\ \text{mmol m}^{-2}\ \text{d}^{-1}$ over sea ice, with smaller values over snow-covered ice (Fig. 8b).
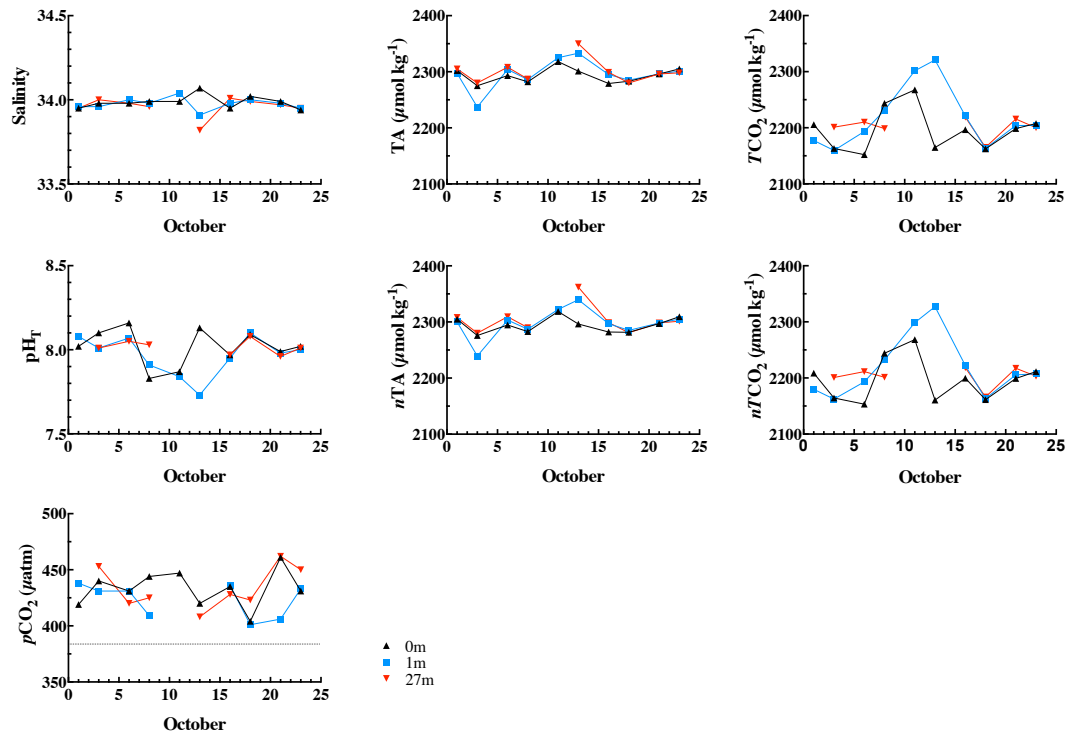
Figure 7. Evolution of salinity, pH_T, TA (in µmol kg^{-1}), nTA (TA normalized to a salinity of 34, in µmol kg^{-1}), calculated $T\text{CO}_2$ (in µmol kg^{-1}) and $nT\text{CO}_2$ ($T\text{CO}_2$ normalized to a salinity of 34, in µmol kg^{-1}), and in situ $p\text{CO}_2$ (in µatm) in the underlying seawater at the ice-water interface and 1 and 27 m below the ice-water interface. The dotted line represents the atmospheric $p\text{CO}_2$ in 2007.
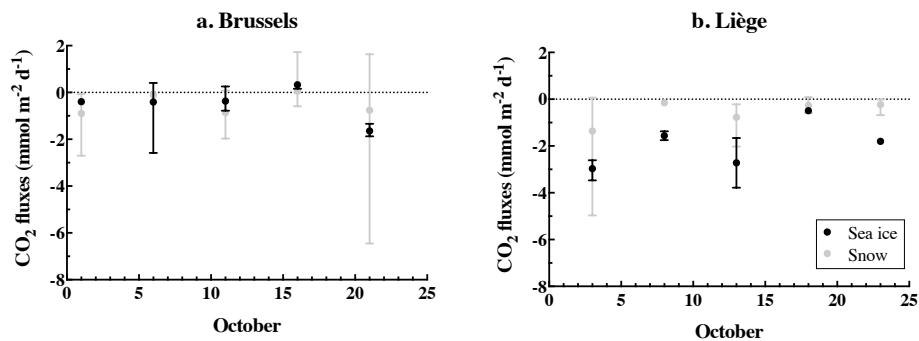

Figure 8. CO_2 fluxes (in mmol m^{-2} d^{-1}) measured over sea ice and snow for the Brussels and Liège sites.

4   Discussion

4.1   Impact of atmospheric forcing and snow thickness on the physical properties of the ice cover

At the beginning of the sampling period the ice cover at stations Brussels and Liège were nearly isothermal. Subsequently, successive warm and cold events associated with passing atmospheric fronts (Fig. 3) affected the temperature gradient within the ice cover significantly. At both sites, the fluctuations in ice temperature occurred mainly in the top 40 cm (Fig. 4). The high brine salinities associated with the cold ice temperature at the top of the ice resulted in an un-

stable salinity gradient within the ice cover (Fig. 4). This may have initiated overturning of brine and the mixing with underlying seawater, with brine moving downward through the ice cover to be replaced by underlying seawater moving upward (Lewis et al., 2011). To confirm this hypothesis, Lewis et al. (2011) reported presence of dissolution features observed on freshly extracted ice cores and thick sections as well as under-ice photographs clearly showing brine drainage at the ice bottom. Brine convection is driven by the density difference between high-salinity brine in the ice and the seawater underneath. Its onset and strength can be described by the mushy-layer Rayleigh numbers (Ra) (Wettlaufer et al., 1997). Ra numbers provided by Brabant (2012)

suggest that brine drainage occurred at the Brussels site between 1 and 6 October ($Ra > 10$) and between 11 and 16 October ($6 < Ra < 7$), which is also confirmed by vertical nutrient distribution in the sea ice (Brabant, 2012). At the Liège site, thicker snow muted thermal fluctuations within the sea ice, reducing the magnitude of changes in brine volume and salinity. Hence, the variations in brine salinity and in the resulting density gradient were more moderate at Liège (Fig. 4), resulting in a lower Ra (Brabant, 2012). It is also possible that some natural intra-site variability within the sea ice existed at the two sampling locations. Given the textural evidence of dynamic processes at Liège (Lewis et al., 2011), one might intuit that variation within salinity especially would be greater at that location, but this was not observed. Lewis et al. (2011) suggested that snow thickness was a key component in regulating the heat fluxes and morphological changes in the sea ice during our study. The ice at the Brussels site had little snow accumulation (Fig. 2) and larger temperature changes than the Liège site (Fig. 4), where the snow cover was thicker and insulated the underlying sea ice cover. Indeed, snow has a low thermal conductivity, about an order of magnitude lower than that of sea ice, and therefore acts as a thermal insulator (Massom et al., 2001).

The presence of a thick snow cover also provided overburden that resulted in negative freeboard (Fig. 2). The negative freeboard observed at the Liège site toward the end of our study, associated with a permeable sea ice cover with an interconnected brine network, caused flooding of the ice surface and formed a saline slush layer (Lewis et al., 2011). Nutrient distribution data in the sea ice further confirmed that flooding occurred (Brabant, 2012).

4.2 Physical controls on inorganic carbon in sea ice

Larger sea ice temperatures changes observed at the Brussels site were associated with generally higher brine salinities (Figs. 4 and 5); higher TA, $T\text{CO}_2$, and in situ $p\text{CO}_2$; and lower pH_T (Fig. 5) compared to the Liège site. These differences were expected because most solute concentrations increase with brine salinity, which also decreases CO_2 solubility (Papadimitriou et al., 2004). As the temperature changes were mainly observed in the upper layer of the ice cover, the differences in salinity, TA, pH_T, $T\text{CO}_2$, and $p\text{CO}_2$ between the upper and lower brine samples were greater at Brussels than at Liège (Fig. 5). However, it is surmised that vertical redistribution of brine between 1 and 6 October homogenized brine salinity, TA, pH_T, $T\text{CO}_2$, and $p\text{CO}_2$ between the two sackhole depths sampled on 6 October. Sea ice temperature decreased between 11 and 16 October, increasing the upper brine salinity and TA (Fig. 5), while the brine volume shrank below the 5 % level (Fig. 4), which in theory should indicate impermeability of the sea ice (Golden et al., 2007) at that thickness, isolating the upper brine layer from those below. Therefore, large differences were observed in salinity, TA, $T\text{CO}_2$, and pH_T between the upper layer and lower brine

samples. At Liège, thermal fluctuations in the ice cover were limited by thicker snow cover, resulting in small differences in salinity, TA, pH_T, $T\text{CO}_2$, and in situ $p\text{CO}_2$ between the upper and lower brine sample depths (Fig. 5).

Brine $p\text{CO}_2$ and, to a lesser extent, bulk ice $p\text{CO}_2$ both seem to follow the observed cyclical variations in the ice temperatures (Fig. 6), indicating that the dilution–concentration effect in large part controls the $p\text{CO}_2$. As the ice cover cooled, the $p\text{CO}_2$ increased slightly (e.g., on 6 and 16 October at the Brussels site and on 18 October at the Liège site; Figs. 4 and 5). Conversely, $p\text{CO}_2$ dropped as temperatures rose (e.g., on 11 and 21 October at Brussels and on 23 October at Liège). Because $p\text{CO}_2$ is highly dependent on temperature, the changes in both brine and bulk ice $p\text{CO}_2$ were larger at the Brussels site than at the Liège site (due to the increased insulation provided by the snow cover at the latter). In addition, greater changes in brine volume content throughout the ice column at the Brussels site (Fig. 4) led to more variability in brine $p\text{CO}_2$ than in the bulk ice due to the effects of brine dilution–concentration (Fig. 6). At the Liège site, the $p\text{CO}_2$ variations were limited by small variations in ice temperature under the thicker snow cover (Fig. 4). Surface flooding on 18 and 23 October might have hydrostatically forced high-$p\text{CO}_2$ seawater laterally or upward through the ice matrix. An increase of the in situ brine $p\text{CO}_2$ and TA was observed on 18 October, but these parameters decreased on 23 October (Figs. 5–6). Therefore, the TA and $p\text{CO}_2$ fluctuations observed between 18 and 23 October could also be solely explained by the changes in the thermal regime (cooling and then warming). Brine salinity seems to be the main control on the brine carbonate system; both nTA and $nT\text{CO}_2$ from both stations were relatively constant through most of the sampling period. The small scatter in the $nT\text{CO}_2$ concentrations could simply be due to errors in calculating $nT\text{CO}_2$ from TA and pH_T. Further, the general agreement between the measured and calculated brine $p\text{CO}_2$ values (Fig. 5) seems to support the assumption that the equilibrium constants are valid at subzero temperatures and high salinities (Marion, 2001; Delille et al., 2007). Only on 1 October did the measured and calculated brine $p\text{CO}_2$ values differ substantially, possibly because of errors in any of the measured parameters on that first day of sampling.

The in situ brine $p\text{CO}_2$ values are more variable than those in bulk ice (Fig. 6). Sampling brine using the sackhole technique provides the advantage of a direct in situ measurement, but the origin of the brine that collects in the sackhole is unknown, and only brine that can move easily within the ice matrix is sampled. In addition, sackholes are subject to air–sea exchange during sampling, so the low-$p\text{CO}_2$ brine could well have absorbed at least some CO_2 from the air above it before we completed our measurements. Brine collected using the sackhole technique represents interconnected liquid brine inclusions, in the form of relatively large brine channels susceptible to mixing with the underlying, high-$p\text{CO}_2$ seawater due to the flooding or other types of vertical re-

distribution. In comparison, our bulk ice pCO_2 analyses address brine at a well-defined location within the sea ice and include both brines and gas bubbles trapped within the ice matrix. It should be stressed that small isolated brine pockets trapped and isolated in the ice matrix are not sampled using the sackhole technique but are nevertheless included in the bulk ice pCO_2 measurement. In addition, the sackhole technique has a poor resolution as it integrates brine through the all sackhole depth, while the resolution of the bulk ice pCO_2 is significantly better as the measurement is performed on a ice sample size of (4 cm × 4 cm × 4.5 cm). On the other hand, the relatively small size of the bulk ice pCO_2 sample might result in not including a (fast-responding) brine channel, the latter typically being several centimeters apart. Therefore, changes in bulk ice pCO_2 values are less variable, reflecting mostly internal melting due to temperature and resultant salinity changes in the ice cover. However, we assumed that microstructure changes due to cooling–warming processes during storage do not have any significant impact to our measurements. Sackhole brine samples highlight rapid changes in the brine network such as cooling/warming events in the ice, input of high-pCO_2 seawater or from brine convection, and possible contamination from contact with the atmosphere during the 10–60-minute collection time window.

4.3 Biological controls on carbon dynamics within sea ice

Dumont (2009) and Brabant (2012) presented a complete description of the distribution and concentration of organic matter, including chlorophyll a (e.g., Fig. 9) in sea ice at both the Brussels and Liège sites. The vertical Chl a distributions were more variable at the Liège site than at Brussels, but neither site showed clear variations in Chl a associated with the changes in pCO_2, save for during the flooding event at Liège from 18 to 23 October, which increased Chl a and pCO_2. However, the presence of biology may overall contribute to the low pCO_2 measured on both sea ice and brine samples. The persistent opposite trends of the Chl a and pCO_2 profiles at Liège might reflect this contribution.

4.4 Antarctic sea ice as a springtime sink of atmospheric CO_2 – comparison with the Arctic

The bulk ice pCO_2 values observed during the present study in the Antarctic are within the same range as those few records existing in the Arctic at Barrow, Alaska (Geilfus et al., 2012b), and Resolute Bay, Canada (Geilfus et al., 2014) (Fig. 10a and b), where sampling also included melting, nearly isothermal first-year landfast sea ice in late spring. Higher pCO_2 values were reported from early spring sea ice at Barrow (Geilfus et al., 2012b) and from SW Greenland (Crabeck et al., 2014). Albeit based on limited data, Antarctic sea ice may have lower pCO_2 values than Arctic sea ice at the same ice temperature (Fig. 10b and c, one-way ANOVA;
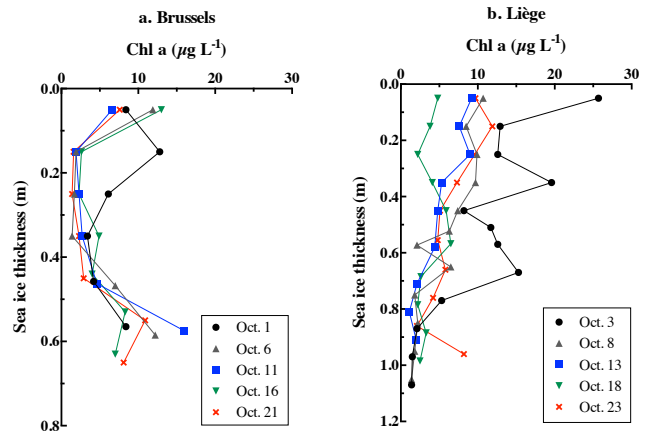

Figure 9. Profiles of Chl a concentration within bulk sea ice at the Brussels and Liège sites, adapted from Dumont (2009).

$F_{1,210} = 30.73$, $p < 0.001$); however, differences in the sea ice texture and dynamical forcing between the two poles are important and may have substantial effects on permeability (and therefore fluxes) and should be further investigated. It is noteworthy that the observed range of concentrations suggests that Antarctic sea ice becomes undersaturated in CO_2 relative to the atmosphere early in the winter–spring transition and reaches levels not observed in Arctic sea ice until much later in the spring decay process (Geilfus et al., 2012a, b, 2014; Crabeck et al., 2014).

The bulk ice pCO_2 data were collected at different times of the year in the Arctic and in the Antarctic (early to late spring) under different temperature and salinity conditions. Therefore we looked at the relationship between the bulk ice pCO_2 and the brine volume (Fig. 10d). At low brine volumes (due to low T and/or high S) the bulk ice pCO_2 is high, while at high brine volumes (due to high T and/or low S) the bulk ice pCO_2 is low (Fig. 10d). It should also be noted that, both in the Arctic and in the Antarctic, spring sea ice can become undersaturated in CO_2 while the underlying seawater is supersaturated with respect to the atmosphere (Fig. 7) (Papakyriakou and Miller, 2011).

During this study, we observed a net uptake of atmospheric CO_2 by the snow and sea ice at both sites. This uptake was on the same order of magnitude as previous fluxes reported over Antarctic sea ice during the austral summer by Delille (2006) and Nomura et al. (2013) and over Arctic sea ice by Semiletov et al. (2004), Nomura et al. (2010a, b), and Geilfus et al. (2012a, 2013, 2014), using similar chamber techniques. At the Brussels site, fluxes measured over snow were similar to those measured over bare ice, suggesting the thin snow cover had a limited impact on CO_2 exchange between the atmosphere and sea ice. At the Liège site, thicker snow cover reduced the magnitude of the fluxes. The snow cover could have acted as a buffer between the ice and the atmosphere, as suggested by Miller et al. (2011). However, in contrast to
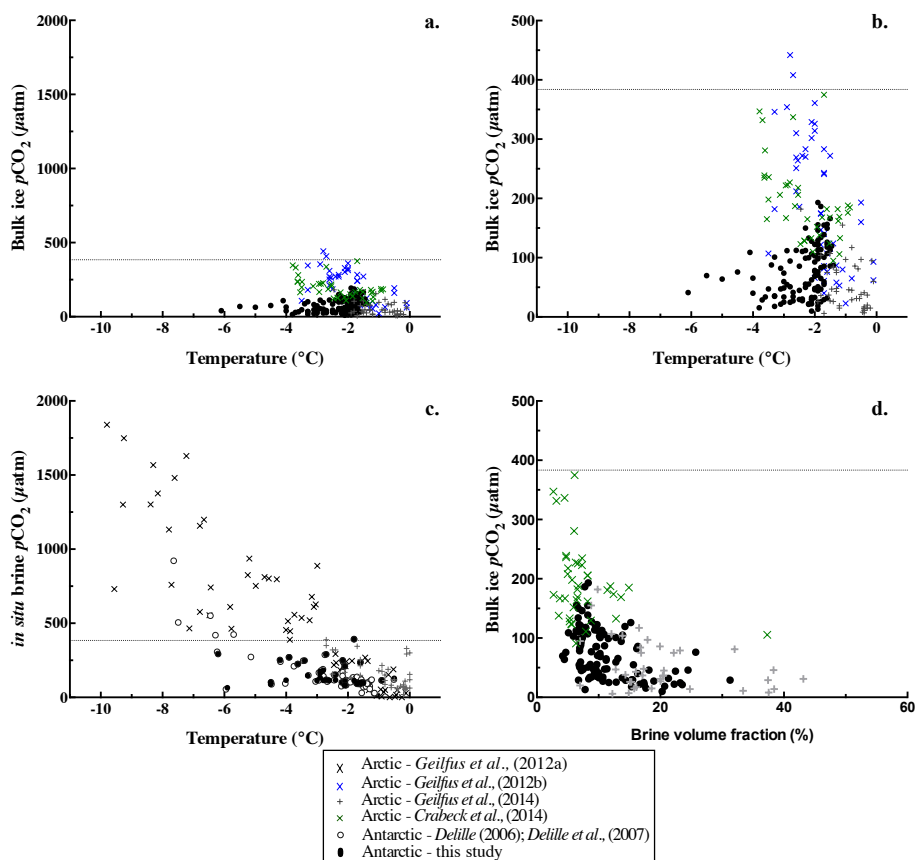
Figure 10. (a) The relationships between bulk ice $p\mathrm{CO_2}$ (in µatm) and temperature measured in Antarctic (this study) and Arctic (Geilfus et al., 2012b, 2014; Crabeck et al., 2014) sea ice; **(b)** zoom-in on the data from **(a)**; **(c)** the relationships between in situ brine $p\mathrm{CO_2}$ (in µatm) and brine temperature in the Antarctic (this study; Delille, 2006; Delille et al., 2007) and Arctic sea ice (Geilfus et al., 2012a); **(d)** relationship between the bulk ice $p\mathrm{CO_2}$ (in µatm) and the brine volume fraction (in %) measured in Antarctic (this study) and Arctic (Geilfus et al., 2012b, 2014; Crabeck et al., 2014) sea ice.

Nomura et al. (2010b), a snow cover thicker than 9 cm did not seem to completely prevent the $\mathrm{CO_2}$ exchanges between the ice and the atmosphere.

5 Conclusions

The inorganic carbon dynamic within sea ice responded swiftly to short-term meteorological events during the SIMA expedition. The succession of warm and cold events impacted the physical properties of the sea ice and its inorganic carbon dynamics. Snow thickness modulated the heat flux to the sea ice, which impacted its salinity and therefore the sea ice carbonate system. Less snow and larger temperature variations created larger variations in brine salinity, TA, $T\mathrm{CO_2}$, and brine and bulk ice $p\mathrm{CO_2}$. In addition, the combination of unstable salinity gradients within the ice cover and episodic warming events initiated vertical brine redistribution at the low-snow site on two occasions, homogenizing brine properties vertically. At the end of the survey, flooding occurred

due to snow loading at the Liège site, bringing high-$p\mathrm{CO_2}$ seawater into the brine system.

During the early spring, sea ice was undersaturated and largely controlled by the brine dilution, although a potential impact of biology could contribute to the overall undersaturation. We highlighted contrasted $p\mathrm{CO_2}$ dynamics in bulk ice measurements as compared to sackhole measurements. The bulk ice $p\mathrm{CO_2}$ values were much less variable, reflecting mostly internal temperature and salinity-driven thermodynamic changes, while $p\mathrm{CO_2}$ variations in sackhole brine reflected rapid transport within an interconnected brine channel network as well as potential exchange with the atmosphere and underlying surface waters.

At both sampling sites, the ice cover acted as a sink for atmospheric $\mathrm{CO_2}$, even despite episodic flooding by supersaturated seawater. Thus, during early spring the inorganic carbonate system in the sea ice of the Bellingshausen Sea behaved as a transition layer between the ocean and the atmosphere, reacting to atmospheric forcing and from episodic interactions with the seawater.

References

Brabant, F.: Physical and biogeochemical controls on the DMS/P/O cycle in Antarctic sea ice, Universite Libre de Bruxelles, Bruxelles, 300 pp., 2012.

Copin Montégut, C.: A new formula for the effect of temperature on the partial pressure of carbon dioxide in seawater, Mar. Chem., 25, 29-37, 1988.

Cox, G. F. N. and Weeks, W. F.: Equations for determining the gas and brine volumes in sea-ice samples, J. Glaciol., 29, 306–316, 1983.

Crabeck, O., Delille, B., Thomas, D., Geilfus, N.-X., Rysgaard, S., and Tison, J.-L.: CO$_2$ and CH$_4$ in sea ice from a subarctic fjord under influence of riverine input, Biogeosciences, 11, 6525–6538, doi:10.5194/bg-11-6525-2014, 2014.

Delille, B.: Inorganic carbon dynamics and air-ice-sea CO$_2$ fluxes in the open and coastal waters of the Southern Ocean, Université de Liège, Liège, 296 pp., 2006.

Delille, B., Jourdain, B., Borges, A. V., Tison, J. L., and Delille, D.: Biogas (CO$_2$, O_2, dimethylsulfide) dynamics in spring Antarctic fast ice, Limnol. Oceanogr., 52, 1367–1379, 2007.

Delille, B., Vancoppenolle, M., Geilfus, N. X., Tilbrook, B., Lannuzel, D., Schoemann, V., Becquevort, S., Carnat, G., Delille, D., Lancelot, C., Chou, L., Dieckmann, G. S., and Tison, J.-L.: Southern Ocean CO$_2$ sink: the contribution of the sea ice, J. Geophys. Res.-Oceans, 119, 6340–6355, doi:10.1002/2014JC009941, 2014.

Dickson, A. G. and Millero, F. J.: A comparison of the equilibrium constants for the dissociation of carbonic acid in seawater media, Deep-Sea Res. Pt. II, 34, 1733–1743, 1987.

Dieckmann, G. S. and Hellmer, H. H.: The importance of Sea Ice: An Overview, in: Sea Ice, second edition, edited by: Thomas, D. N. and Dieckmann, G. S., Wiley-Blackwell, Oxford, 1–22, 2010.

DOE: Handbook of methods for the analysis of the various parameters of the carbon dioxide system in sea water, version 2, edited by: Dickson, A. G. and Goyet, C., ORNL/CDIAC-74, http://cdiac.ornl.gov/oceans/DOE_94.pdf (last access: 19 December 2014), 1994.

Dumont, I.: Interactions between the microbial network and the organic matter in the Southern Ocean: impacts on the biological carbon pump, Université Libre de Bruxelles, Bruxelles, 202 pp., 2009.

Eicken, H.: Salinity Profiles of Antarctic Sea Ice - Field Data and Model Results, J. Geophys. Res.-Oceans, 97, 15545–15557, 1992.

Frankignoulle, M.: Field-Measurements of Air Sea CO$_2$ Exchange, Limnol. Oceanogr., 33, 313–322, 1988.

Frankignoulle, M. and Borges, A. V.: Direct and indirect pCO$_2$ measurements in a wide range of pCO$_2$ and salinity values (the Scheldt estuary), Aquat. Geochem., 7, 267–273, 2001.

Geilfus, N. X., Carnat, G., Papakyriakou, T., Tison, J. L., Else, B., Thomas, H., Shadwick, E., and Delille, B.: Dynamics of pCO$_2$ and related air-ice CO$_2$ fluxes in the Arctic coastal zone (Amundsen Gulf, Beaufort Sea), J. Geophys. Res.-Oceans, 117, C00G10, doi:10.1029/2011JC007118, 2012a.

Geilfus, N. X., Delille, B., Verbeke, V., and Tison, J. L.: Towards a method for high vertical resolution measurements of the partial pressure of CO$_2$ within bulk sea ice, J. Glaciol., 58, 287–300, 2012b.

Geilfus, N. X., Carnat, G., Dieckmann, G. S., Halden, N., Nehrke, G., Papakyriakou, T., Tison, J. L., and Delille, B.: First estimates of the contribution of CaCO$_3$ precipitation to the release of CO$_2$ to the atmosphere during young sea ice growth, J. Geophys. Res., 118, 224–255, doi:10.1029/2012JC007980, 2013.

Geilfus, N.-X., Galley, R. J., Crabeck, O., Papakyriakou, T., Landy, J., Tison, J.-L., and Rysgaard, S.: Inorganic carbon dynamics of melt pond-covered first year sea ice in the Canadian Arctic, Biogeosciences Discuss., 11, 7485–7519, doi:10.5194/bgd-11-7485-2014, 2014.

Gleitz, M., vd Loeff, M. R. D., Thomas, N., Dieckmann, G. S., and Millero, F. J.: Comparison of summer and winter inorganic carbon, oxygen and nutrient concentrations in Antarctic sea ice brine, Mar. Chem., 51, 81–91, 1995.

Golden, K. M., Ackley, S. F., and Lytle, V. I.: The percolation phase transition in sea ice, Science, 282, 2238–2241, 1998.

Golden, K. M., Eicken, H., Heaton, A. L., Miner, J., Pringle, D. J., and Zhu, J.: Thermal evolution of permeability and microstructure in sea ice, Geophys. Res. Lett., 34, L16501, doi:10.1029/2007GL030447, 2007.

Gran, G.: Determination of the equivalence point in potentiometric titration, Analyst, 77, 661–671, 1952.

Leppäranta, M. and Manninen, T.: The brine and gas content of sea ice with attention to low salinities and high temperatures, Rep., Finnish Institute of Marine Research, Helsinki, 15 pp., 1988.

Lewis, M. J., Tison, J. L., Weissling, B., Delille, B., Ackley, S. F., Brabant, F., and Xie, H.: Sea ice and snow cover characteristics during the winter-spring transition in the Bellingshausen Sea: An overview of SIMBA 2007, Deep-Sea Res. Pt. II, 58, 1019–1038, 2011.

Marion, G. M.: Carbonate mineral solubility at low temperatures in the Na-K-Mg-Ca-H-Cl-SO$_4$-OH-HCO$_3$-CO$_3$-CO$_2$-H$_2$O system, Geochim. Cosmochim. Acta, 65, 1883–1896, 2001.

Massom, R. A., Eicken, H., Haas, C., Jeffries, M. O., Drinkwater, M. R., Sturm, M., Worby, A. P., Wu, X., Lytle, V. I., Ushio, S., Morris, K., Reid, P. A., Warren, S. G., and Allison, I.: Snow on Antarctic Sea ice, Rev. Geophys., 39, 413–445, 2001.

Mehrbach, C., Culberson, C. H., Hawley, J. E., and Pytkowicz, R. M.: Measurements of the apparent dissociation constants of carbonic acid in seawater at atmospheric pressure, Limnol. Oceanogr., 18, 897–907, 1973.

Miller, L. A., Chierici, M., Johannessen, T., Noji, T. T., Rey, F., and Skjelvan, I.: Seasonal dissolved inorganic carbon variations in the Greenland Sea and implications for atmospheric CO$_2$ exchange, Deep-Sea Res. Pt. II, 46, 1473–1496, 1999.

Miller, L. A., Papakyriakou, T., Collins, R. E., Deming, J., Ehn, J., Macdonald, R. W., Mucci, A., Owens, O., Raudsepp, M., and Sutherland, N.: Carbon Dynamics in Sea Ice: A Winter Flux Time Series, J. Geophys. Res.-Oceans, 116, C02028, doi:10.1029/2009JC006058, 2011.

Nomura, D., Eicken, H., Gradinger, R., and Shirasawa, K.: Rapid physically driven inversion of the air-sea ice CO$_2$ flux in the seasonal landfast ice off Barrow, Alaska after onset surface melt, Cont. Shelf Res., 30, 1998–2004, 2010a.

Nomura, D., Yoshikawa-Inoue, H., Toyota, T., and Shirasawa, K.: Effects of snow, snow-melting and re-freezing processes on air-sea ice CO$_2$ flux, J. Glaciol., 56, 262–270, 2010b.

Nomura, D., Granskog, M. A., Assmy, P., Simizu, D., and Hashida, G.: Arctic and Antarctic sea ice acts as a sink for atmospheric CO$_2$ during periods of snowmelt and surface flooding, J. Geophys. Res.-Oceans, 118, 6511–6524, doi:10.1002/2013JC009048, 2013.

Papadimitriou, S., Kennedy, H., Kattner, G., Dieckmann, G. S., and Thomas, D. N.: Experimental evidence for carbonate precipitation and CO$_2$ degassing during sea ice formation, Geochim. Cosmochim. Acta, 68, 1749–1761, 2004.

Papadimitriou, S., Thomas, D. N., Kennedy, H., Haas, C., Kuosa, H., Krell, A., and Dieckmann, G. S.: Biogeochemical composition of natural sea ice brines from the Weddell Sea during early austral summer, Limnol. Oceanogr., 52, 1809–1823, 2007.

Papakyriakou, T. and Miller, L.: Springtime CO$_2$ exchange over seasonal sea ice in the Canadian Arctic Archipelago, Ann. Glaciol., 52, 215–224, 2011.

Parmentier, F.-J. W., Christensen, T. R., Sørensen, L. L., Rysgaard, S., McGuire, A. D., Miller, P. A., and Walker, D. A.: The impact of lower sea-ice extent on Arctic greenhouse-gas exchange, Nat. Clim. Change, 3, 195–202, doi:10.1038/nclimate1784, 2013.

Rysgaard, S., Glud, R. N., Sejr, M. K., Bendtsen, J., and Christensen, P. B.: Inorganic carbon transport during sea ice growth and decay: A carbon pump in polar seas, J. Geophys. Res.-Oceans, 112, C03016, doi:10.1029/2006JC003572, 2007.

Rysgaard, S., Bendtsen, J., Delille, B., Dieckmann, G. S., Glud, R. N., Kennedy, H., Mortensen, J., Papadimitriou, S., Thomas, D. N., and Tison, J. L.: Sea ice contribution to the air-sea CO(2) exchange in the Arctic and Southern Oceans, Tellus B, 63, 823–830, 2011.

Rysgaard, S., Glud, R. N., Lennert, K., Cooper, M., Halden, N., Leakey, R. J. G., Hawthorne, F. C., and Barber, D.: Ikaite crystals in melting sea ice – implications for pCO$_2$ and pH levels in Arctic surface waters, The Cryosphere, 6, 901–908, doi:10.5194/tc-6-901-2012, 2012.

Rysgaard, S., Wang, F., Galley, R. J., Grimm, R., Notz, D., Lemes, M., Geilfus, N.-X., Chaulk, A., Hare, A. A., Crabeck, O., Else, B. G. T., Campbell, K., Sørensen, L. L., Sievers, J., and Papakyriakou, T.: Temporal dynamics of ikaite in experimental sea ice, The Cryosphere, 8, 1469–1478, doi:10.5194/tc-8-1469-2014, 2014.

Semiletov, I. P., Makshtas, A., Akasofu, S. I., and Andreas, E. L.: Atmospheric CO$_2$ balance: The role of Arctic sea ice, Geophys. Res. Lett., 31, L05121, doi:10.1029/2003GL017996, 2004.

Thomas, D. N. and Dieckmann, G. S.: Sea Ice – An introduction to its physics, biology, chemistry and geology, in: Sea Ice, edited by: Thomas, D. N. and Dieckmann, G. S., 2nd Edn., Science, Oxford, UK, Wiley, Blackwell, London, p. 621, 2010.

Tison, J. L., Worby, A., Delille, B., Brabant, F., Papadimitriou, S., Thomas, D., de Jong, J., Lannuzel, D., and Haas, C.: Temporal evolution of decaying summer first-year sea ice in the Western Weddell Sea, Antarctica, Deep-Sea Res. Pt. II, 55, 975–987, 2008.

Vancoppenolle, M., Timmermann, R., Ackley, S. F., Fichefet, T., Goosse, H., Leonard, K. C., Lieser, J., Nicolaus, M., Papakyriakou, T., and Tison, J.-L.: Assessment of radiation forcing data sets for large-scale sea ice models in the Southern Ocean, Deep-Sea Res. Pt. II, 58, 1237–1249, 2011.

Weeks, W. F. (Ed.): On Sea Ice, Fairbanks, University of Alaska Press, Alaska, 664 pp., 2010.

Wettlaufer, J. S., Worster, M. G., and Huppert, H. E.: Natural convection during solidification of an alloy from above with application to the evolution of sea ice, J. Fluid Mech., 344, 291–316, 1997.

Zemmelink, H. J., Delille, B., Tison, J. L., Hintsa, E. J., Houghton, L., and Dacey, J. W. H.: CO$_2$ deposition over the multi-year ice of the western Weddell Sea, Geophys. Res. Lett., 33, L13606, doi:10.1029/2006GL026320, 2006.